Phys Chem Minerals (2004) 31: 353–359
DOI 10.1007/s00269-004-0403-l

ORIGINAL PAPER

G. Shen · W. Sturhahn · E. E. Alp · J. Zhao
T. S. · Toellner · V. B. Prakapenka · Y. Meng
H.-R. Mao

Phonon density of states in iron at high pressures and high temperatures

Received: 8 November 2003/Accepted: 23 April 2004

Abstract The phonon density of states (DOS) in iron has been measured in situ by nuclear resonance inelastic X-ray scattering (NRIXS) at high pressures and high temperatures in a resistively heated diamond anvil cell. The DOS data provide a variety of thermodynamic and elastic parameters essential for characterizing iron at depth in the Earth interior, such as average sound velocity, Debye temperature, atomic mean square displacement, average kinetic energy, vibrational entropy and specific heat. The NRIXS data were collected at 6, 20, and 29 GPa and at temperatures up to 920 K. Temperatures were directly determined from the measured spectra by the ratio of intensities of the phonon creation/annihilation side bands that are determined only by the Boltzmann factor. The change of the DOS caused by the structural transition from α-Fe to ε-Fe is small and not resolvable within the experimental precision. However, the phonon energies in γ-Fe are clearly shifted to lower values with respect to α- and ε-Fe. The temperature dependence of derived thermodynamic parameters is presented and compared with those obtained by Debye's model. The Debye temperatures that best describe the data decrease slightly with increasing temperature.

Keywords Phonon density of states · Nuclear resonance inelastic X-ray scattering · Diamond anvil cell · Iron

G. Shen (✉) · V. B. Prakapenka
Center for Advanced Radiation Sources,
University of Chicago, Chicago, IL 60637, USA
e-mail: shen@cars.uchicago.edu

W. Sturhahn · J. Zhao · T. S. Tollenner
Advanced Photon Source, Argonne National Laboratory,
Argonne, IL 60439, USA

Y. Meng · H.-R. Mao
Geophysical Laboratory, Carnegie Institution of Washington,
Washington DC 20015, USA

Y. Meng · H.-R. Mao
HPCAT, Advanced Photon Source,
Argonne National Lab, Argonne, IL 60439, USA

Introduction

The lattice dynamics of materials is commonly described by phonons. Measuring phonon dispersion relations and phonon density of states (DOS) at in situ high pressures and high temperatures can have great importance in geophysics. In fact, thermodynamic and elastic properties of relevant candidate constituents of the Earth interiors, which can be derived from DOS, are necessary to interpret global geophysical and geochemical evidence. Iron is abundant in the Earth and is the dominant component in the core. It transforms from a *bcc* phase (α-Fe) to an *fcc* phase (γ-Fe) at moderate pressures and temperatures and to a *hcp* phase (ε-Fe) at higher pressures (Shen et al. 1998; Uchida et al. 2001). The lattice dynamics of iron has been extensively investigated in both experimental and theoretical studies. Dispersion relations have been measured in single-crystal α-Fe using inelastic neutron scattering under ambient conditions (Minkiewicz et al. 1967) and at pressures up to 10 GPa (Klotz and Braden 2000). Single-crystal measurements provide information on dispersion, single-crystal elastic tensor, and anisotropy. With proper averaging, dispersion relations can also be used for calculating phonon DOS. However, these measurements cannot be performed on the high-pressure polymorph ε-Fe because the sample becomes polycrystalline at the onset of the phase transition. With the recently developed nuclear resonant inelastic X-ray scattering (NRIXS) technique (Seto et al. 1995; Sturhahn et al. 1995), the phonon DOS can be directly obtained from polycrystalline samples. Measurements on polycrystalline α-Fe (Seto et al. 1995) and the DOS extraction from α-Fe and iron-bearing compounds (Sturhahn et al. 1995) demonstrated the feasibility of this method for the study of lattice dynamics. The NRIXS measurements on ε-Fe were performed up to 42 GPa (Lübbers et al. 2000), and up to 153 GPa with improved X-ray focusing techniques and energy resolutions (Mao et al. 2001). The dispersion of longitudinal acoustic phonons of polycrystalline ε-Fe

was measured by inelastic X-ray scattering (IXS) up to 110 GPa (Fiquet et al. 2001). The extrapolation of the dispersion curve to low energies provided values for the longitudinal sound velocity (V_p). Light-scattering measurements also provide information of the lattice dynamics of iron. Raman spectra for ε-Fe were measured to 152 GPa (Merkel et al. 2000), where the Raman-active mode corresponding to an optical phonon E_{2g} was correlated with a transverse acoustic phonon, providing an approximation of the shear constant C_{44}.

All these high-pressure measurements were performed at room temperature. For characterizing materials at depth in the Earth interior, it is desirable for such measurements to be possible under high temperatures. The temperature dependence of phonons in iron at ambient pressure has been studied using neutron scattering (Vallera 1981; Satija et al. 1985; Zarestky and Stassis 1987), nuclear forward scattering (Bergmann et al. 1994), and NRIXS (Chumakov et al. 1996). Recently, Debye–Waller factors, which give information about atomic mean square displacement, have been determined through Rietveld refinement from X-ray diffraction data for iron collected at high pressures and high temperatures using a resistively heated diamond anvil cell (DAC) (Dubrovinsky et al. 2001). In this paper, we report the results of NRIXS measurements on iron at simultaneously high pressures and high temperatures. The temperature dependence of the phonon DOS and the derived thermodynamic and elastic parameters of iron at high pressures are presented and evaluated in terms of Debye's model (Debye 1912).

Experimental

We employed the internal resistance technique to heat the samples to high temperatures in a DAC (Mao et al. 1987). An iron foil (95% pure isotopically enriched in ^{57}Fe) was loaded in a boron insert Be gasket (Lin et al. 2003; Shen et al. 2003). The sample configuration is schematically shown in Fig. 1. The Pt foil electrodes and iron sample (resistance element) were insulated from the Be gasket by layers of Al_2O_3 powder. A DC power supply provided electric current through the iron sample. The heating power was calculated from applied voltages and currents. To know the heating power–temperature relationship at each pressure, we preheated the sample two or three times to a temperature of ~ 1200 K, which was measured by a spectroradiometric system at GeoSoilEnviroCARS (Shen et al. 2001). The DAC and heating assembly were then moved to the experimental station for NRIXS measurements. We assumed that temperature would change linearly with electric power (Zha and Bassett 2003), and we adjusted the electrical power level to the desired temperature range. Final temperatures were determined from the collected NRIXS data (see below). Pressures were measured before and after the high-temperature NRIXS measurements using the ruby pressure scale (Mao et al. 1986).

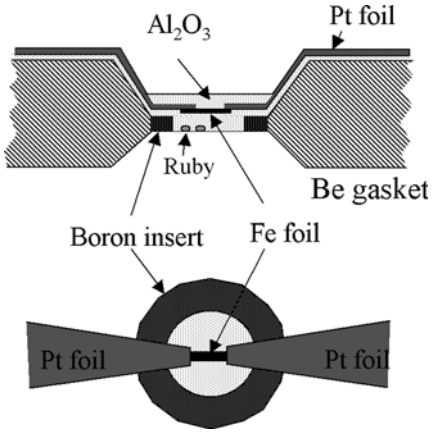

Fig. 1 Schematics of a resistively heated iron foil in the diamond anvil cell. The iron strip was about 25 μm in width and 5–10 μm in thickness

The NRIXS measurements were performed at the synchrotron beam line 3ID at the Advanced Photon Source. The details of the experimental setup for the diamond cell have been reported elsewhere (Mao et al. 2001). The synchrotron radiation was monochromatized to 2 meV bandwidth and tuned ± 110 meV around the nuclear transition energy of 14.4125 keV in steps of 0.6 meV. Synchrotron radiation is emitted in short pulses, and if the energy is close to the nuclear transition energy, nuclei are excited, and delayed emission of X rays within the lifetime of the excited nuclear state (141 ns) can be observed. In the experiment, we recorded only the yield of a secondary radiation of Fe–$K_{\alpha,\beta}$ fluorescence in the time window between synchrotron pulses while tuning the energy of the incident X-ray pulses. This time-discrimination method removes all nonnuclear scattering of the X rays very effectively. The phonon excitation probability density $S(E)$ is then obtained directly from the measured data by proper normalization, and the partial phonon DOS can be extracted by a mathematical procedure (Sturhahn 2000). A detailed theoretical treatment of incoherent nuclear resonant scattering and the properties of $S(E)$ has been given earlier (Sturhahn and Kohn 1999).

The NRIXS data were collected at 6, 20, and 29 GPa and at temperatures up to 920 K. The typical counting rate in the phonon side bands was 0.4 Hz at room temperature and 1.2 Hz at a temperature of 920 K. The typical accumulation time for each NRIXS spectrum was about 12 h. The data were evaluated using the PHOENIX software (Sturhahn 2000).

Results and discussion

NRIXS data

Figure 2 shows a typical excitation probability density $S(E)$ directly normalized from the inelastic scattering intensity $I(E) = AS(E)$. The value of $S(E)dE$ gives the

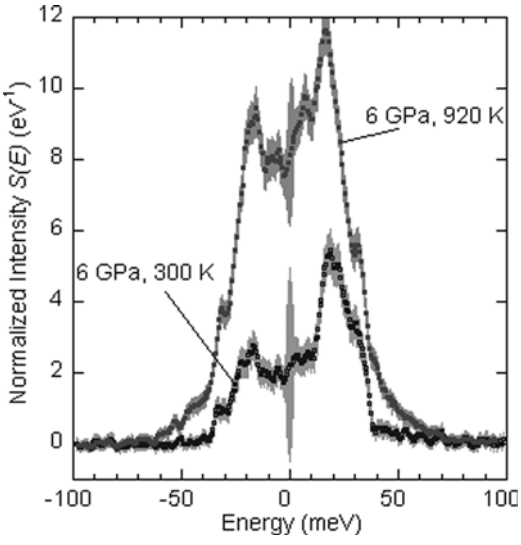

Fig. 2 The phonon excitation probability density $S(E)$ determined from NRIXS data at 6 GPa and at two different temperatures. Energy zero corresponds to the nuclear transition energy of 14.4125 keV, positive (negative) energies indicate the region of phonon creation (annihilation). High temperature has two obvious effects: the increase of overall probability density and the growth in the side band of phonon annihilation

probability that the resonant nucleus can be excited by X-rays in the energy range $(E,E+dE)$. Since phonon states with any momentum allowed by the dispersion relations contribute equally to the probability, NRIXS provides momentum-averaged information. The intensity of the inelastic side band is proportional to $(1\text{-}f_{\mathrm{LM}})$, where f_{LM} is the Lamb–Mössbauer factor or the probability of recoilless absorption. From $S(E)$, f_{LM} can be directly determined (Sturhann et al. 1995; Sturhahn and Chumakov 1999). The intensity increases with temperature, reflecting the decrease in the recoilless fraction f_{LM}. The lattice average kinetic energy can also be derived directly from NRIXS data (Sturhahn and Chumakov 1999; Sturhann 2004). The side band at positive energies represents phonon creation, while the side band at negative energies arises from phonon annihilation. The ratio is given by the Boltzmann factor:

$$S(E) = e^{\beta E} S(-E), \tag{1}$$

where $\beta = 1/(k_{\mathrm{B}}T)$ is the inverse temperature, and k_{B} the Boltzmann constant. The temperature of the sample can be determined from the Bolzmann factor.

Temperature determination from NRIXS data

For DAC experiments with external heating techniques, temperatures are usually measured by thermocouples. With internal heating methods, such as laser heating and resistive heating, temperatures above 900–1000 K are measured by thermal radiation signals fitted to the Planck radiation law (Boehler 1986; Shen et al. 2001). However, there are currently no satisfactory methods available for temperature determination at temperatures below 900–1000 K with internally heated DAC. We address this issue successfully by determining the temperature from the NRIXS data using the Boltzmann factor.

From Eq. (1), the data pairs $[S(\pm E)]$ provide us with temperatures that can be averaged. We determine an average temperature using the relationship:

$$\int S(E)dE = \int e^{\beta E} S(-E)dE, \tag{2}$$

where the integration range in our case is 5meV < E < ∞. This 5-meV cutoff value is chosen to avoid contributions from the tails of the elastic peak. Apparently from Eq.(2), the temperature determination depends on the spectral shape of a particular system and statistical accuracy in experiments. An error analysis retaining only first-order terms results in the following expression:

$$\frac{\delta\beta}{\beta} = \frac{1}{\sqrt{A}} \frac{\sqrt{\int (1+e^{\beta E}) S(E)dE}}{\int e^{\beta E} \beta E S(E)dE}. \tag{3}$$

Here, A is the normalization factor; the integration ranges are 5 meV < E < ∞. The trivial effect of increased statistical accuracy, e.g., by longer collection times resulting in larger values of A, is now separated from the effects of spectral shape. Note that $S(E)$ is temperature-dependent and that the uncertainty is a complicated function of spectral shape and temperature itself. At the low-temperature limit $\beta \to \infty$, the uncertainty will grow without bound. This behavior is evident because the measured signal $S(E)$ simply disappears when zero temperature is approached. The high-temperature limit is described by $\beta \to 0$, and Eq. (3) takes the form:

$$\frac{\delta\beta}{\beta} = \frac{1}{\sqrt{A}} \frac{\sqrt{\int 2S(E)dE}}{\int \beta E S(E)dE}. \tag{4}$$

The normalization of the positive-valued function $S(E)$ leads to a finite numerator. The denominator will disappear as $\sqrt{\beta}$ because the integral $\int ES(E)dE$ behaves like the square root of the total energy, which is proportional to $1/\beta$. Thus, we have the following asymptotic form

$$\frac{\delta\beta}{\beta} \propto \frac{1}{\sqrt{A\beta}} \text{ or } \frac{\delta T}{T} \propto \frac{\sqrt{T}}{\sqrt{A}}. \tag{5}$$

This means that for high temperatures the uncertainty in temperature will increase without bound as well, and is proportional to $\sqrt{T}$. However, the increase may be compensated by improving the statistical accuracy (by the factor $\frac{1}{\sqrt{A}}$). Particularly at high temperatures, counting rates are higher (see, for example, Fig. 2), and help to improve counting statistics. In combination with longer collecting times, good statistics ($\sqrt{A}$) might overcome the term $\sqrt{T}$ and give reasonable accuracy for temperature measurements.

From the data in this study, the values of A were found to be around 30000. Temperature uncertainties calculated by Eq.(3) are listed in Table 1, with a level typically at 5–10%.

Table 1 Derived thermodynamic and elastic parameters from NRIXS measurements[a]

P^b (GPa)	T^c (K)	f_{LM}	C_{vib} (k_B)	S_{vib} (k_B)	E_k (meVatom^{-1})	θ_D^d (K)	V_{av} (kms^{-1})	F_m (Nm^{-1})
0	300	0.7951(6) *0.794(1)*	2.722(9)	3.133(9)	42.54(18) *42.51(15)*	430(2)	3.54(1)	174(2)
6.0(5)	300	0.772(3) *0.798(11)*	2.75(7)	3.30(4)	42.1(8) *42.8(3)*	407(5)	3.21(8)	155(6)
6.0(5)	920(28)	0.403(2) *0.399(39)*	2.97(6)	6.68(8)	117(1) *121(2)*	372(2)	2.73(1)	144(3)
20(1)	720(24)	0.590(4) *0.615(35)*	2.94(11)	5.55(11)	92(2) *97(5)*	435(3)	3.21(2)	182(7)
29(2)	300	0.852(4) *0.848(12)*	2.61(7)	2.66(6)	44(1) *43(4)*	526(7)	3.98(9)	253(17)
29(2)	430(18)	0.782(6) *0.789(25)*	2.80(8)	3.68(12)	59(2) *60(6)*	498(6)	3.71(4)	249(19)
29(2)	720(35)	0.656(7) *0.615(35)*	2.93(8)	5.25(23)	95(3) *97(3)*	485(5)	3.65(7)	235(15)

[a]All quantities are calculated from the derived phonon DOS, except those in italics that are calculated directly from NRIXS spectra using sum rules. Numbers in parentheses denote uncertainties at the last digit(s)

[b]Pressures were determined using the ruby scale; uncertainties reflect pressure variations from an area of 30 μm in diameter; pressure change before and after the high-temperature NRIXS measurements was found to be less than 1 GPa

[c]Temperatures were determined from the measured NRIXS spectra by the ratio of intensities of the phonon creation/annihilation side bands

[d]The Debye temperatures are calculated from f_{LM}, using (6) and the relation $f_{LM} = e^{-k^2<\Delta x^2>}$

Phonon density-of-states

The phonon DOS was extracted from measured inelastic scattering spectra by using the PHOENIX software, which follows the data analysis procedure described by Hu et al. (1999) and Sturhahn 2000). The multi-phonon contributions and the central elastic peak were subtracted from the measured spectrum. The remaining single-phonon contribution gives the phonon DOS. The results of DOS spectra for all experimental conditions are summarized in Fig. 3. The derived thermodynamic parameters are listed in Table 1.

In general, the spectral features of the DOS (Fig. 3) are shifted to higher energies with increasing pressure and to lower energies with increasing temperature. However, the DOS spectrum collected at 6 GPa and 920 K is shifted to lower energies with respect to α-Fe at ambient conditions. At this pressure and temperature the stable phase of iron is γ-Fe (Zhang and Guyot 1999). The shift to lower energy is due to the α- to γ-Fe phase transition. The spectrum at 6 GPa and 300 K (Fig. 4) was collected after the sample was heated at 920 K for 12 h. As reported by Zhang and Guyot (1999) γ-Fe could be temperature-quenchable and coexists with α-Fe in this pressure range (referred to as quench in Fig. 4). The DOS for the quenched sample in Fig. 4 shows that it contains large portions of the γ-Fe phase. Overall, the DOS of γ-Fe in this study is consistent with the DOS of γ-Fe precipitates in a Cu matrix (Tsunoda et al. 2002), and with the data of γ-Fe that were calculated from the dispersion relations determined at 1480 K and at ambient pressure (Zarestky and Stassis 1987). Under ambient conditions, we obtained a similar DOS pattern from a steel with *fcc* structure with the same experimental setup (Fig. 4).

It is interesting to note that the DOS change caused by structural transition from α-Fe to ε-Fe is small and not resolvable within experimental precision (Lübbers et al. 2000; Mao et al. 2001), but there is a clear difference in DOS between γ-Fe and α- or ε-Fe. Considering the structural similarity between γ-Fe and ε-Fe, both having closely packed structures, the difference in lattice dynamics is remarkable and warrants further studies. The shift in DOS spectra of γ-Fe naturally influences all derived thermodynamic and elastic parameters (Table 1). For example, the *fcc* iron (or alloys) has systematically lower Debye temperatures and average sound velocities than *hcp* iron.

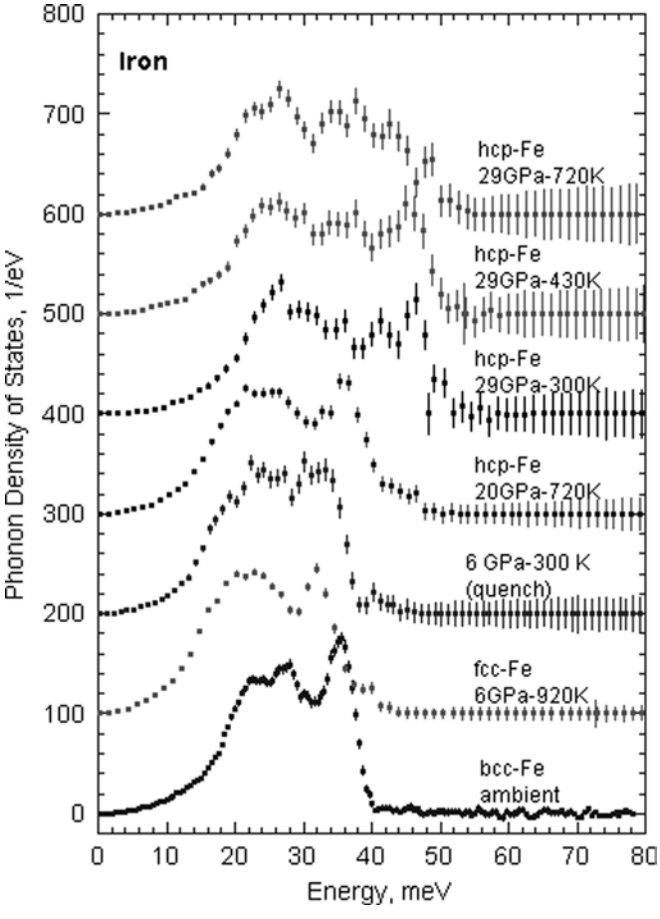

Fig. 3 Summary of phonon density of states determined in this study. Vertical offset is applied for clarity

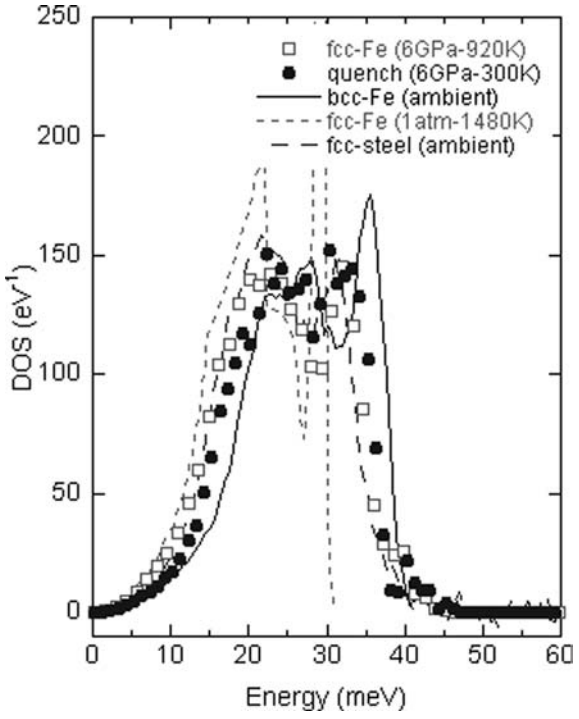

Fig. 4 Phonon density of states of γ-Fe at 6 GPa. The spectra are shifted to lower energies with respect to α-Fe. Inelastic neutron scattering data of γ-Fe at 1480 K and at ambient pressure (Zarestky and Stassis 1987) is shown for comparison. Also plotted is the DOS of an *fcc*-structured stainless steel determined with the same experimental setup

Thermodynamic and elastic parameters

Thermodynamic and elastic parameters were derived from the measured DOS at high pressures and high temperatures. By integration of the DOS, we obtained properties such as vibrational contribution to entropy (S_{vib}) and specific heat (C_{vib}), mean force constant (F_m), vibrational kinetic energy (E_k), Debye temperature (θ_{D}), the Lamb–Mössbauer factor (f_{LM}), the mean square displacement ($\langle \Delta x^2 \rangle$), and average sound velocity (V_{av}) (Table 1). In addition, we calculated vibrational kinetic energy, and Lamb–Mössbauer factor directly from *S(E)* using sum rules as reviewed by Sturhahn and Chumakov, (1999). The agreement of both methods within the accuracy of the data proves the validity of the quasi-harmonic approximation in the pressure–temperature range of this study. Debye temperatures in Table 1 were calculated from f_{LM} values. Values for the Debye sound velocity were obtained from parabolic fits to the low-energy region of the DOS (Hu et al. 2003). The temperature effect on these parameters at 29 GPa is shown in Fig. 5. For comparison, we employed Debye's model, and results are shown as lines in the figure. For the vibrational contribution to entropy and specific heat, there is a reasonable agreement between the obtained data and those from the model at Debye temperature of 500 ± 30 K (Figs. 5A,B). Debye's model can also successfully stretch the data points of the kinetic energy (Fig. 5C). Also plotted in Fig. 5C is the $\frac{3}{2}k_BT$ classical limit. It can be seen that the kinetic energy approaches the classical limit above the Debye temperature. The mean force constant (Fig. 5D) from the Debye model is calculated by $F_m = \frac{9}{10}\frac{k^2}{E_r}k_{\mathrm{B}}^2\theta_{\mathrm{D}}^2$, where k = 7.31 Å^{-1} is the wave vector of the 14.41-keV quanta; $E_r = \frac{h^2k^2}{2M}$ is the recoil energy with M the mass of nuclear isotope. The weak temperature dependence of the mean force constant qualitatively agrees with a harmonic model for the lattice vibrations. Data on mean force constant also indicates that Debye temperatures slightly decrease with increasing temperature. Figure 5E shows data of the average sound velocity (V_{av}) from the low-energy portion of the DOS spectra. Using the molar volume data by Uchida, et al. (2001), V_{av} is calculated from Debye temperatures through the relation $\theta_{\mathrm{D}} = 251.2V^{-\frac{1}{3}}V_{\mathrm{av}}$ where V is the molar volume in cm^3 and V_{av} in kms^{-1}. Again, velocity data indicate that Debye temperatures slightly decrease with increasing temperatures. This decrease is also evidenced from the Lamb–Mössbauer factor (Fig. 5F) and the mean square displacement $\langle \Delta x^2 \rangle$ (Fig. 5G). These two parameters are related by $f_{\mathrm{LM}} = e^{-k^2\langle \Delta x^2 \rangle}$. In Debye's model, the mean square displacement $\langle \Delta x^2 \rangle$ is obtained by the relation (Maradudin et al. 1971):

$$\langle \Delta x^2 \rangle = \frac{6E_r}{k^2 k_B \theta_{\mathrm{D}}}\left[\frac{1}{4} + (\frac{T}{\theta_D})^2 \int_0^{\frac{\theta_D}{T}} \frac{x}{e^x - 1}dx\right]. \quad (6)$$

It appears that Debye's model describes the temperature dependence of thermodynamic parameters moderately well. This is not too surprising for the case of iron, for which it can be assumed that all atoms are mechanically equivalent and that lattice vibrations are well described by acoustic phonons. The small decrease of θ_{D} with increasing temperature is related to anharmonicity effects in the lattice. The Debye temperatures from average sound velocity (the elastic θ_{D}), heat capacity (the calorimetric θ_{D}), and the Lamb–Mössbauer factor are plotted in Fig. 5H. The difference in Debye temperature from various parameters decreases as temperature increases, indicating a more Debye-like lattice at higher temperatures.

Conclusions

Thermodynamic and elastic properties of α-Fe, γ-Fe and ε-Fe phases have been studied using NRIXS at in situ high pressures to 29 GPa and high temperatures to 920 K. Derived properties from the NRIXS data include phonon density of state, vibrational specific heat, vibrational entropy, average kinetic energy, mean force constant, the Lamb–Mössbauer factor, Debye temperature, and average sound velocity. In this study, temperatures were directly determined from the measured NRIXS spectra by the ratios of intensities of the phonon creation/annihilation side bands. It is found

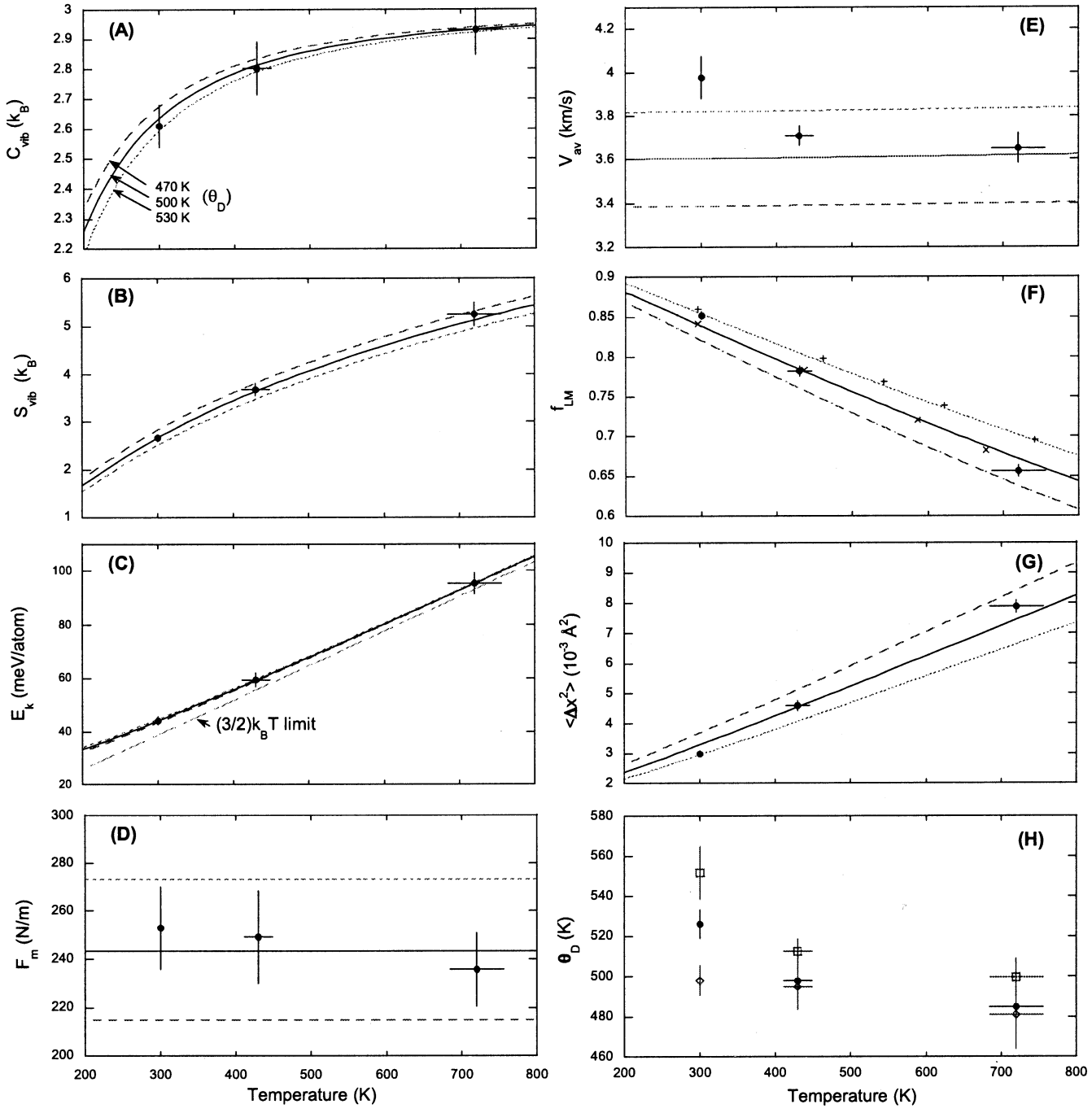

Fig. 5A–H Temperature dependence of thermodynamic and elastic parameters of ε-Fe at 29 GPa. *Lines* are the calculations from Debye's model, with *dashed line* at θ_D = 470 K, *solid line* at 500 K, and *dotted line* at 530 K. **A** Vibrational contribution to specific heat. **B** Vibrational contribution to entropy. **C** Vibrational kinetic energy. **D** Mean force constant. **E** Average sound velocity. **F** Lamb–Mössbauer factor. *Pluses* and *crosses* are from Dubrovinsky et al. (2001) at 34 GPa and 19 GPa, respectively. **G** Mean square displacement. **H** Debye temperatures calculated from different parameters: *squares* from V_{av}, *solid circles* from f_{LM}; diamonds from C_{vib}. It appears that Debye's model describes the temperature dependences of these parameters moderately well. An anharmonicity effect is noticeable, with Debye temperature decreasing as temperature increases

that the change in the phonon DOS caused by the structural transition from α-Fe to ε-Fe is small and not resolvable within experimental precision. However, a clear difference in lattice dynamics is observed for γ-Fe, with its phonon energies shifted to lower values with respect to α-Fe and ε-Fe. Consequently, γ-Fe has systematically lower Debye temperatures and average sound velocities than ε-Fe. Temperature dependence of derived parameters for ε-Fe at 29 GPa can be described by Debye's model moderately well, implying a Debye-like lattice for ε-Fe. The Debye temperatures that best describe the data decrease slightly with increasing temperature.

Acknowledgements This work is supported by NSF-EAR 0229987. Work at Argonne is supported by US Department of Energy, Basic Energy Sciences, under contract no: W-31-109- ENG-38.

References

Bergmann U, Shastri SD, Siddons DP, Batterman BW, Hastings JB (1994) Temperature dependence of nuclear forward scattering of synchrotron radiation in α- ^{57}Fe. Phys Rev (B) 50: 5957–5961

Boehler R (1986). The phase diagram of iron to 430 kbar. Geophy Res Lett 13: 1153–1156

Chumakov AI, Rüffer R, Baron AQR, Grünsteudel H, Grünsteudel HF (1996) Temperature dependence of nuclear inelastic absorption of synchrotron radiation in α-^{57}Fe. Phys Rev (B) 54: R9596–9599

Debye P (1912). Zur Theorie der spezifischen Wärmen. Ann Phys 39: 789–839

Dubrovinsky LS, Dubrovinskaia NA, Le Bihan T (2001) Aggregate sound velocities and acoustic Grüneisen parameter of iron up to 300 GPa and 1200 K. PNAS 98: 9484–9489

Fiquet G, Badro J, Guyot F, Requardt H and Krisch M (2001) Sound velocities in iron to 110 gigapascals. Science 291: 468–471

Hu M, Sturhahn W, Toellner TS, Hession PM, Sutter JP, Alp EE (1999) Data analysis for inelastic nuclear resonant absorption experiments. Nucl Instrum and Methods in Phys Res A, 428: 551–555

Hu M, Sturhahn W, Toellner TS, Mannheim PD, Brown DE, Zhao JY, Alp EE (2003) Measuring velocity of sound with nuclear resonant inelastic x-ray scattering. Phys Rev (B) 67: 094304

Klotz S, Braden M (2000) Phonon dispersion of *bcc* iron to 10 GPa. Phys Rev Lett 85: 3209–3212

Lin JF, Shu JF, Mao HK, Hemley RJ, Shen G (2003) Amorphous boron gasket in diamond anvil cell research. Rev Sci Instru 74: 4732–4736

Lübbers R, Grünsteudel HF, Chumakov AI, Wortmann G (2000) Density of states in iron at high pressure. Science 287: 1250–1253

Mao HK, Xu J, Bell PM (1986) Calibration of the ruby pressure gauge to 800 kbar under quasi-hydrostatic conditions. J Geophys Res 91: 4673–4676

Mao HK, Bell PM, Hadidiacos C (1987) Experimental phase relations of iron to 360 kbar and 1400 C, determined in an internally heated diamond anvil apparatus. In: Manghnani MH, Syono Y (eds.) High-pressure research in mineral physics. Terra Scientific Publishing Company/American Geophysical Union, Tokyo, Washington DC, pp 135–138

Mao HK, Xu J, Struzhkin V, Shu J, Hemley RJ, Sturhahn W, Hu MY, Alp EE, Vocadlo L, Alfè D, Price GD, Gillan MJ, Schwoerer-Böhning M, Häusermann D, Eng P, Shen G, Giefers H, Lubers R, Wortmann G (2001) Phonon density of states of iron up to 153 Gigapascals. Science 292: 914–916

Maradudin AA, Montroll EW, Weiss GH and Ipatova IP, 1971. Theory of lattice dynamics in the harmonic approximation. Solid State Phys Academic Press, New York

Merkel S, Goncharov AF, Mao HK, Gillet P and Hemley RJ, (2000). Raman spectroscopy of iron to 152 gigapascals: implications for Earth's inner core. Science 288: 1626–1629

Minkiewicz VJ, Shirane G, Nathans R (1967) Phonon dispersion relation for iron. Phys Rev 162: 528–531

Satija SK, Comes RP, Shirane G (1985) Neutron scattering measurements of phonons in iron above and below Tc. Phys Rev (B) 32: 3309–3311

Seto M, Yoda Y, Kikuta S, Zhang XW, Ando M (1995) Observation of nuclear resonant scattering accompanied by phonon excitation using synchrotron radiation. Phys Rev Lett 74: 3828–3831

Shen G, Mao HK, Hemley RJ, Duffy TS, Rivers ML (1998) Melting and crystal structure of iron at high pressures. Geophys Res Lett 25: 373–376

Shen G, Rivers ML, Wang Y, Sutton SJ (2001) A laser heated diamond cell system at the Advanced Photon Source for in situ X-ray measurements at high pressure and temperature. Rev Sci Instrum 72: 1273–1282

Shen G, Prakapenka VB, Rivers ML, Sutton SR (2003) Structural investigation of amorphous materials at high pressures using the diamond anvil cell. Rev Sci Instru 74: 3021–3026

Sturhahn W (2000) CONUSS and PHOENIX: Evaluation of nuclear resonant scattering data. Hyperfine Interactions 125: 149–172

Sturhahn W (2004) Nuclear resonant scattering. J Phys. Condens Matter, 16: 497–530

Sturhahn W, Chumakov AI (1999) Lamb–Mössbauer factor and second-order Doppler shift from inelastic nuclear resonant absorption. Hyperfine Interactions 123/124: 803–824

Sturhahn W, Kohn VG (1999) Theoretical aspects of incoherent nuclear resonant scattering. Hyperfine Interactions 123/124: 367–399

Sturhahn W, Toellner TS, Alp EE, Zhang XW, Ando M, Yoda Y, Kikuta S, Seto M, Kimball CW, Dabrowski B (1995) Phonon density of states measured by inelastic nuclear resonant scattering Phys Rev Lett 74: 3832–3835

Tsunoda Y, Kurimoto Y, Seto M, Kitao S, Yoda Y (2002). Phonon density of states of gamma-Fe precipitates in Cu. Phys Rev (B) 66: 214304

Uchida T, Wang Y, Rivers ML, Sutton SR (2001) Stability field and thermal equation of state of ε-iron determined by synchrotron X-ray diffraction in a multianvil apparatus. J. Geophys Res (B)10: 21799–810

Vallera AM (1981) High-temperature phonons in iron. J Phys (C)6: 398–400

Zarestky J, Stassis C (1987) Lattice dynamics of gamma-Fe. Phys Rev (B) 35: 4500–4502

Zha CS, Bassett WA (2003) Internal resistive heating in diamond anvil cell for in situ X-ray diffraction and Raman scattering. Rev Sci Instru 74: 1225–1262

Zhang J, Guyot F (1999) Experimental study of the *bcc–fcc* phase transformations in the Fe-rich system Fe–Si at high pressures. Phys Chem Miner 26: 419–424